Adsorption of star polymers: computer simulations

Post-print of peer-reviewed article published by the Royal Society of Chemistry.
Published article available at: http://dx.doi.org/10.1039/B922988D

Cite as:
Chremos, A., Camp, P. J., Glynos, E., & Koutsos, V. (2010). Adsorption of star polymers: computer simulations. *Soft Matter*, 6(7), 1483-1493.

Manuscript received: 03/11/2009; Accepted: 05/01/2010; Article published: 08/02/2010

Adsorption of star polymers: computer simulations**

A. Chremos,[1,†] P.J. Camp,[1,*] E. Glynos[2,‡] and V. Koutsos[2]

[1]EaStCHEM, School of Chemistry, Joseph Black Building, University of Edinburgh, West Mains Road, Edinburgh, EH9 3JJ, UK.

[2]Institute of Materials and Processes, School of Engineering, and Centre for Materials Science and Engineering, University of Edinburgh, Mayfield Road, Edinburgh, EH9 3JL, U.K.

[†]Current address: Department of Chemical Engineering, Princeton University, Princeton, NJ 08540, USA.

[‡]Current address: Department of Materials Science and Engineering, University of Michigan, Ann Arbor, MI 48109-2136, USA.

[*]Corresponding author; e-mail: philip.camp@ed.ac.uk

[**]This research was supported by the School of Chemistry at the University of Edinburgh through the award of a studentship to A. C.; and by the EPSRC DTA, and the Institute for Materials and Processes in the School of Engineering at the University of Edinburgh, through the award of a studentship to E. G.

Graphical abstract:

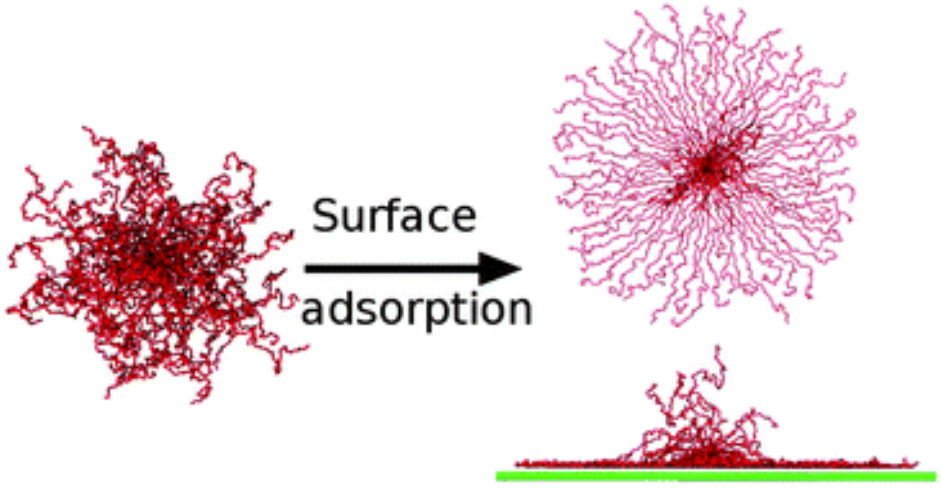

Abstract

The behaviour of star polymers adsorbed on smooth surfaces is studied using coarse-grained bead-spring models and Langevin dynamics simulations. The conformational properties of a single adsorbed star polymer in good-solvent conditions are considered as functions of the functionality (number of arms) f, the number of monomers per arm N, and the monomer-surface interaction energy ε_s. Four conformational regimes are identified: a linear-polymer regime; a two-dimensional star polymer regime; a sombrero regime; and a colloidal regime. The latter three correspond to regimes predicted theoretically by Halperin and Joanny [*J. Phys. II (France)*, 1991, **1**, 623–636]. Solvent effects are explored by dialing in effective attractions between the monomer beads; with decreasing solvent quality, the star polymers adopt more compact, globular structures. Good-solvent to bad-solvent quenches at finite surface coverages are considered; these correspond to established experimental protocols for adsorbing and then drying polymer sub-monolayers on surfaces. The structure of the polymer film is surveyed as a function of surface coverage, f, N, and ε_s, in good-solvent and bad-solvent conditions. The simulated post-quench structures are in good qualitative agreement with those observed in atomic-force microscopy measurements, while the simulated pre-quench structures shed light on the microscopic mechanisms of film formation. This study draws together much of what is known about surface-adsorbed star polymers from theory, simulation, and experiment.

1. Introduction

A star polymer is a single molecule composed of f flexible polymer chains, or *arms*, tethered to a core particle; f is called the *functionality*. The conformational statistics of a single star polymer in dilute solution are well understood from the standard blob model introduced by Daoud and Cotton[1] and further developed in the work of Birshtein *et al.*[2,3] In the Daoud–Cotton model, the star is represented by concentric shells of blobs. For f = 1 and 2 a star resembles a linear polymer meaning that for low functionalities, it exhibits highly aspherical conformations.[4,5] As the functionality is increased, asphericity drops significantly and the star becomes stiffer and more spherical like a soft colloid.[6–8] In short, star polymers bridge two very important fields of soft matter – polymers and colloids – which have long histories and important industrial applications.

Of recent interest is how star polymers in solution behave in the proximity of a substrate. One important example is how star polymers act as depleting agents for colloidal particles, and how they can be used for controlling colloidal aggregation to produce desired ordered structures.[9–11] From theoretical[12–16] and simulation[17–19] studies of star polymers on flat surfaces, different structural regimes can be identified, each determined by the attractive interaction strength (δ) between a

monomer unit and the surface: (i) for small δ, the conformational statistics of the star polymer are essentially those of the free molecule in dilute solution (*colloidal* regime); (ii) for large δ, the star polymer is strongly adsorbed on the surface, and all of its arms are in contact with the surface leading to quasi-two dimensional conformational statistics (*2D star* regime); and (iii) for intermediate δ, a non-trivial 'sombrero' structure is predicted theoretically,[15] where f_{ads} arms are strongly adsorbed on the surface, and the remaining $f–f_{ads}$ free arms are in contact with the solution (*sombrero* regime). This list can be supplemented by a *linear* regime, applicable at very low functionalities, where the arms on the surface behave essentially independent of one another. In the sombrero regime, the conformational statistics are expected to be intermediate between two-dimensional and three-dimensional limiting cases; this case has not, to our knowledge, been observed in simulation studies. One of the goals of this work is to map out the different regimes, and represent them on a phase diagram in the plane of functionality f and number of monomers per arm N. To the best of our knowledge, we provide the first simulations of the sombrero structure predicted by Halperin and Joanny.[15]

In recent work by our groups , the physisorption and self-assembly of linear[20] and star[21] polymers on smooth surfaces were examined using atomic-force microscopy (AFM). In a typical experiment, a polymer solution was prepared in good-solvent conditions at concentrations well below the critical overlap volume fraction (ϕ^*), resulting in well-separated polymers in solution and hence precluding any strong degree of structural ordering prior to adsorption. Polymer (sub-)monolayers were formed by exposing a smooth surface (such as mica) to the polymer solution. The surface was then placed in a good solvent for several hours and extensively rinsed with good solvent to remove any non-adsorbed polymer . Finally, the samples were dried gently under a stream of nitrogen and subsequently imaged in air by AFM in tapping mode to investigate the structures resulting from the good solvent-to-bad solvent quench. The glass-transition temperature of the polymers was more than 100 K below room temperature and so all of the observed structures should be at, or close to, thermodynamic equilibrium. Depending on the polymer molecular weight, architecture, and concentration, very different surface structures can be obtained. This protocol is somewhat related to that reported by Kiriy *et al.*,[22] in which starpolymers were adsorbed from dilute solutions in various good and selective solvents , dried by rapid solvent evaporation , and then characterised in AFM measurements.

A full report on the experimental investigation of linear polymers is in preparation[20] and a simulation study yielding insight on the as-yet-unpublished experimental results has already appeared.[23] Using the same experimental procedure, the adsorption of star polybutadiene on to mica from toluene solution has been studied. The functionality and concentration of star polymers can be used to control a crossover between the aforementioned polymer and colloidal regimes, being distinguished by characteristic cluster topologies, sizes, and surface coverage.[21] An aim of this work is to reproduce,

and gain insight on, the experimentally observed adsorption regimes using Langevin dynamics simulations of coarse-grained bead-spring models of star polymers .

In the past, the bulk properties of star polymers and the crossover between the polymer and colloidal structural regimes have been examined experimentally, theoretically, and with computer simulations. In particular, computer simulations have helped to confirm the predictions of the Daoud–Cotton model and its scaling laws.[24–26] Simulations have also been used to obtain the effective interactions between star polymers , which can be used to coarse-grain the whole star polymer as one ultra-soft particle;[27] this technique has yielded valuable insights on the bulk-phase properties of star polymers , including the phase diagram.[27] Despite numerous simulation studies of star polymers , their detailed behaviour in the proximity of an attractive surface is largely unexplored. To the best of our knowledge, simulation work has been limited to many-arm star polymers tethered to surfaces by the core particles,[17–19] and to lattice models of physisorbed $f = 3$ star polymers .[28,29] It should be noted, however, that the behaviour of star-branched polyelectrolytes on oppositely charged surfaces in the presence of counterions has been thoroughly surveyed using computer simulations.[30] The so-called 'starfish', 'antenna', 'anemone', 'jellyfish', and 'sea urchin' structures observed in this system are somewhat similar to those described above.

This paper reports a simulation study of physisorbed star polymers . We use Langevin dynamics simulations of coarse-grained bead-spring models to gain insight on the results from polymer adsorption experiments.[21] The outline of this study is as follows. Firstly, we study the properties of isolated adsorbed polymers (vanishing surface coverage) in both good-solvent and bad-solvent conditions. We compare our simulated isolated-polymer structures under bad-solvent conditions to those inferred from AFM experiments on systems at low surface coverages.[21] Secondly, we deal with many polymers on a surface in both good-solvent and bad-solvent conditions, and compare the resulting sub-monolayer films with those produced in experiments.[21] The paper is organized as follows. Section II contains details of the coarse-grained polymer model, and the simulation methods. The results are presented in section III, and section IV concludes the paper.

2. Simulation and methods

A. Simulation model

In this work a star polymer is modelled with f polymer chains, which are bonded to a core particle. Each chain is composed of N beads of equal size and mass, connected by bonds. The size of the core particle may be larger than the size of the beads, especially for $f > 32$, to allow space for the arms. The core size was kept as small as possible and was insignificant compared to the star's overall

dimensions. A star of *f* arms and *N* beads per arm will be abbreviated by the notation *f*/*N*. Such bead-spring models of linear and star polymers were first introduced and employed in simulations by Grest and co-workers.[24,25,31,32] In this work, *N* beads are connected to form a chain using a non-linear finitely extensible (FENE) potential between neighbouring beads, given by

$$V_{\mathrm{FENE}}(r) = -\frac{1}{2}kR_0^2 \ln\left(1 - \frac{r^2}{R_0^2}\right). \quad (1)$$

Here r is the bead-bead separation, R_0 is the maximum possible (bonded) bead-bead separation, and k is a spring constant. In this study we use parameters from earlier work,[24] namely $R_0 = 1.5\sigma$ and $k = 30\varepsilon/\sigma^2$; ε and σ are the energy and range parameters, respectively, for the non-bonded interactions to be defined next.

Non-bonded interactions operate between all pairs of beads, and are derived from a composite potential devised by Steinhauser.[33] The potential is a combination of three terms. The first contribution is the purely repulsive Weeks–Chandler–Andersen (WCA) potential,[34] which is a Lennard–Jones potential cut and shifted at the position of the minimum, $r_{\mathrm{min}} = 2^{1/6}\sigma$:

$$V_{\mathrm{WCA}}(r) = \begin{cases} 4\varepsilon\left[\left(\frac{\sigma}{r}\right)^{12} - \left(\frac{\sigma}{r}\right)^{6}\right] + \varepsilon & r \le r_{\mathrm{min}} \\ 0 & r > r_{\mathrm{min}} \end{cases}. \quad (2)$$

To represent the attractive interactions, the WCA potential is shifted back down in the range $0 \le r \le$ rmin by a square-well (SW) potential

$$V_{\mathrm{SW}}(r) = \begin{cases} -\lambda\varepsilon & 0 < r \le r_{\mathrm{min}} \\ 0 & r > r_{\mathrm{min}} \end{cases} \quad (3)$$

where λ reflects the solvent quality (to be discussed below). To interpolate the potential smoothly between $-\lambda\varepsilon$ at $r = r_{\mathrm{min}}$ and 0 at a cut-off distance$r_{\mathrm{cut}} > r_{\mathrm{min}}$, we add the term

$$V_{\mathrm{cos}}(r) = \begin{cases} \frac{1}{2}\lambda\varepsilon[\cos(\alpha r^2 + \beta) - 1] & r_{\mathrm{min}} < r \le r_{\mathrm{cut}} \\ 0 & r > r_{\mathrm{cut}} \end{cases} \quad (4)$$

where α and β satisfy the conditions $\alpha r_{\mathrm{min}}^2 + \beta = \pi$ and $\alpha r_{\mathrm{cut}}^2 + \beta = 2\pi$. The cosine form of the potential also means that the force $-\mathrm{d}V_{\mathrm{cos}}/\mathrm{d}r = 0$ at $r = r_{\mathrm{cut}}$. Following earlier work,[33] $r_{\mathrm{cut}} = 3\sigma/2$ for which the appropriate parameters are

$$\alpha = \frac{4\pi}{9 - 4\sqrt[3]{2}} = 3.173\ 072\ 868, \tag{5}$$

$$\beta = 2\pi - \frac{9}{4}\alpha = -0.856\ 228\ 645. \tag{6}$$

The final, non-bonded potential is $V(r) = V_{WCA} + V_{SW}(r) + V_{cos}(r)$. The parameter λ controls the depth of the potential well at $r = r_{min}$, and provides a convenient measure of the solvent quality. In a good solvent , the effective bead-bead interactions are purely repulsive; this corresponds to$\lambda = 0$. In a bad solvent , the bead-bead interactions are attractive, and this behaviour can be modelled with $\lambda = 1$; this corresponds to the same well depth as in the Lennard–Jones potential, which has been used frequently in the past. θ-solvent conditions – under which the chain statistics are very similar to those for an ideal (non-interacting) chain – are reproduced by $\lambda = 0.646$.[33]

For simulations involving a surface, an additional effective bead-surface potential is used,[32] based on integrating the Lennard–Jones interactions arising from a homogeneous distribution of sites within the surface. The potential is

$$V_s(z) = \frac{2\pi\varepsilon_s}{3}\left[\frac{2}{15}\left(\frac{\sigma}{z}\right)^9 - \left(\frac{\sigma}{z}\right)^3\right] \tag{7}$$

where z is the perpendicular distance of the bead from the surface, and ε_s controls the strength of the bead-surface attraction.

Langevin dynamics are used to simulate the bead-spring polymer chains, in which the system is coupled to a heat bath, corresponding physically to solvent . In addition to the conservative forces arising from the interaction potentials described above, each bead will feel random and frictional forces mimicking the solvent surrounding the bead. Thus the equations of motion for bead i are given by

$$m\frac{\mathrm{d}^2\boldsymbol{r}_i}{\mathrm{d}t^2} = -\nabla_{\boldsymbol{r}_i}V - m\Gamma\frac{\mathrm{d}\boldsymbol{r}_i}{\mathrm{d}t} + \boldsymbol{W}_i(t) \tag{8}$$

where m is the bead mass, Γ is the friction coefficient, $\boldsymbol{W}_i(t)$ represents the Brownian forces of the solvent acting on the bead, and $V = \sum_{i<j}V_{ij}$ is the total interaction potential. $\boldsymbol{W}_i(t)$ is represented by Gaussian white noise satisfying the fluctuation-dissipation theorem[35]

$$\langle \boldsymbol{W}_i(t)\cdot\boldsymbol{W}_j(t')\rangle = 6k_BTm\Gamma\delta_{ij}\delta(t-t') \tag{9}$$

where k_B is Boltzmann's constant, and T is the temperature. The Einstein relation leads to a diffusion constant for an isolated bead of $D_0 = k_BT/m\Gamma$. Further details are given in ref. 31.

Simulations are performed in an $L \times L \times H$ cuboidal box with periodic boundary conditions in all three directions and the minimum-image convention applied. The box dimension in the z direction is set to a large but finite value of $H = 200\sigma$, and the surface is represented by a structureless, $L \times L \times l$ solid slab with a thickness l no less than the maximum range of interaction between beads. To control the surface bead density, L takes on values of 80σ through to 180σ, which are always large enough for polymers in their natural conformations to avoid interacting with their own periodic images. The simulation conditions mean that the polymers are at finite density within the simulation cell , and so there is an equilibrium state where the polymers are adsorbed. In principle, the polymers could adsorb on either face of the slab, but they cannot interact with each other because l is larger than the interaction range, and H is much larger than typical polymer dimensions (as measured by the radius of gyration, R_g); hence, the two surfaces are essentially isolated from one another. In practice, initial configurations are prepared by placing the polymers on one face of the slab, and all subsequent measurements are made for that one surface. Simulated properties are reported here in reduced units defined in terms of m, ε, and σ. The equations of motion were integrated using the velocity-Verlet algorithm with a time step $\delta t = 0.007\tau$, where $\tau = \sqrt{m\sigma^2/\varepsilon}$ is the basic unit of time. In all cases, the reduced temperature $k_BT/\varepsilon = 1$, and the reduced friction coefficient $\Gamma\tau = 1$.

3. Results and discussion

We have studied four different situations using Langevin dynamics simulations: (i) the behaviour of an isolated star polymer on a surface in good-solvent conditions ($\lambda = 0$); (ii) the behaviour of an isolated star polymer on a surface in various solvent qualities ($0 < \lambda \leq 1$); (iii) the behaviour of many star polymers on a surface in good-solvent conditions ($\lambda = 0$); and (iv) many star polymers in bad-solvent conditions ($\lambda = 1$). The good-solvent conditions correspond to the experimental situation before the bad-solvent quench, while the bad-solvent conditions mimic the dried state of the experimental system which is probed in AFM experiments. Star polymers with functionalities in the range $2 \leq f \leq 128$ and three different chain lengths ($N = 25$, 50, and 100), on different surfaces having bead-surface energy parameters $\varepsilon^*_s = \varepsilon_s/\varepsilon = 0.4$, 0.6, 0.8 and 1.0 have been studied; in the case of many polymers, a range of surface coverages was also explored.

A. An isolated star in good solvent

Some earlier studies have focused on the conformations of isolated star polymers with the cores tethered to a surface.[17–19] In the case of repulsive or marginally attractive surfaces, and with the core particle tethered on the surface, the configuration of a star polymer is similar to that of a bulk star polymer with twice as many arms.[36] In the case of strongly attractive surfaces, core-adsorbed star polymers resemble two-dimensional polymers . To the best of our knowledge, however, very little simulation work has been carried out on many-arm star polymers adsorbed on attractive surfaces without the core tethered to the surface. Sikorski studied a lattice model of $f = 3$ star polymers , concentrating on a comparison with linear and ring polymers ,[28] and on the equilibrium dynamics.[29] Here, simulations are used to study the surface effects on a physisorbed star polymer , and to survey the different structural regimes controlled by the functionality f, the arm length N, and the bead-surface energy ε^*_s. Model parameters are chosen which correspond to the physisorption regime, meaning that the interaction between a bead and the surface is of order k_BT; adsorption is favoured because of the large number of contacts between individual beads and the surface.

All isolated polymer simulations began with a star polymer being placed in good-solvent conditions ($\lambda = 0$) and close enough to the surface for adsorption to occur. The required equilibration time depended on f, N and ε^*_s. Equilibration was complete within $2 \times 10^5 \delta t$ for the smallest molecules and up to $8 \times 10^6 \delta t$ for the largest. Subsequently, the measured properties were averaged over a production run of $4 \times 10^6 \delta t$. Snapshots of some equilibrated polymer conformations are shown in Figure 1.

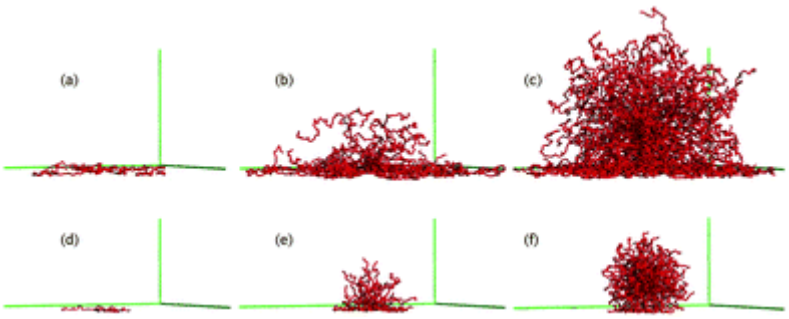

Figure 1. Snapshots of isolated f/N star polymers (f is functionality, N is arm length) adsorbed on the surface in good-solvent conditions ($\lambda = 0$) and with bead-surface energy $\varepsilon^*_s = 0.6$: (a) 4/100; (b) 32/100; (c) 128/100; (d) 4/25; (e) 32/25; (f) 128/25.

Figure 2 shows how the behaviour of the average maximum height of the star $\langle h \rangle$, and the average height of the core particle $\langle h_{\mathrm{core}} \rangle$, vary with the functionality. The results are plotted in units of R_c, the root mean square centre-end distance of a star polymer in bulk:

$$R_c = \left\langle \frac{1}{f} \sum_{\text{end points } i}^{f} (\mathbf{r}_i - \mathbf{r}_{\mathrm{core}})^2 \right\rangle^{1/2} . \qquad (10)$$

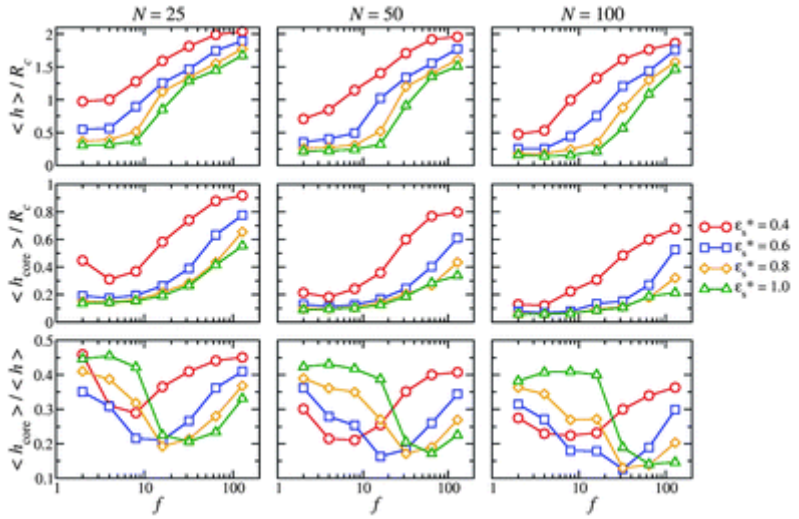

Figure 2. Dimensions of an adsorbed star polymer with arm lengths $N = 25$ (left column), $N = 50$ (middle column), and $N = 100$ (right column) in good-solvent conditions ($\lambda = 0$): (top row) average height of the star $\langle h \rangle$ in units of the root mean square centre-end distance R_c [Eq. (10)]; (middle row) average core height $\langle h_{\mathrm{core}} \rangle$ in units of R_c; (bottom row) ratio $\langle h_{\mathrm{core}} \rangle$ / $\langle h \rangle$.

$\langle h \rangle$ /R_c shows how the overall polymer structure is affected by the star's interaction with the surface, while $\langle h_{\mathrm{core}} \rangle$ /R_c reflects how much the centre of the star is pulled down on to the surface. The general trend is for the ratios to increase with increasing f, approaching the values 2 and 1, respectively, these limits corresponding to the bulk structure.

The ratio $\langle h_{\mathrm{core}} \rangle$ / $\langle h \rangle$ describes the relation between the height of the star and the position of its core. For low values of f the ratio $\langle h_{\mathrm{core}} \rangle$ / $\langle h \rangle$ has values slightly less then 0.5, which means that the core is located slightly lower than the mid-height of the molecule. The ratio has higher values and closer to 0.5 for more attractive surfaces because the bead-surface interactions disfavour dangling tails

and large loops, which otherwise would increase $\langle h \rangle$. Thus even though the core particle is close to the surface – as indicated by $\langle h_{\text{core}} \rangle$ – the ratio increases for more attractive surfaces.

Above a threshold value of f (which increases with increasing N or ε^*_s) the ratio $\langle h \rangle / R_c$ increases significantly, with $\langle h_{\text{core}} \rangle / R_c$ following the lead but at a different rate. This happens because as f is increased the number of arms effectively saturates the region near the core of the star, where the whole structure is essentially flat on the surface. At the threshold functionality, $\langle h_{\text{core}} \rangle / \langle h \rangle$ significantly drops because any new arms will find the surface too crowded and will therefore point away from the surface, thus increasing $\langle h \rangle$. There are two characteristic conformational features in this regime; the first one is that the adsorbed arms form a disk lying on the surface, and the second feature is that, due to crowding, some arms form a central fountain [Figure 1(b) and (e)]. In fact, this conformation was predicted theoretically by Halperin and Joanny, and was christened the "sombrero" structure.[15] As far as we are aware, this structure has not been reported in earlier simulation studies.

Beyond the threshold functionality there is an increase of $\langle h_{\text{core}} \rangle / R_c$, because the area around the core particle becomes more crowded and that lifts the core particle away from the surface. At higher values of f, the ratios $\langle h \rangle / R_c$ and $\langle h_{\text{core}} \rangle / R_c$ continue to increase towards values of 2 and 1, respectively; the ratio $\langle h_{\text{core}} \rangle / \langle h \rangle$ reaches a minimum and continues with an increase towards 0.5. The star polymer essentially starts to regain its bulk shape and features, and the effects of the surface are reduced. The star polymer now starts to resemble either a hemispherical droplet [Figure 1(c)] or a spherical droplet [Figure 1(f)] due to the osmotic pressure within its volume. In other words the star behaves like a soft-colloid, since it is stiff enough to resist the flattening effects of the attractive surface forces. This effect is also seen in AFM experiments[21] albeit in the post-quench, bad-solvent regime; this issue is addressed specifically in the next section. The variation of $\langle h_{\text{core}} \rangle / \langle h \rangle$ with ε^*_s for high-functionality star polymers is in reverse of what is observed in the linear-polymer regime ($f \simeq 2$); a lower bead-surface energy means less structural perturbation to the star polymer , and hence $\langle h_{\text{core}} \rangle / \langle h \rangle$ tends to 0.5 from below.

To understand further the behaviour of the adsorbed star polymer, attention is drawn to the radius of gyration,

$$\langle R_g^2 \rangle = \frac{1}{N_b^2} \left\langle \sum_{i=1}^{N_b} \sum_{j=i}^{N_b} (\mathbf{r}_i - \mathbf{r}_j)^2 \right\rangle \qquad (11)$$

where $N_b = Nf + 1$ is the total number of beads. It is well known that for star polymers in solution $\langle R^2_g \rangle \sim N^{2\nu} f^{1-\nu}$, where ν is the Flory exponent.[1] In good-solvent conditions $\nu \simeq 3/5$, therefore $\langle R^2 \rangle$

$\sim N^{6/5} f^{2/5}$. Far from a surface, the average shape of a star is spherical. But near a surface, it is necessary to consider the different dimensions of the star with respect to the surface. Therefore, we resolve the vector $\mathbf{r}_i - \mathbf{r}_j$ in Eq. (11)in to components perpendicular ($\perp$) and parallel ($\parallel$) to the surface, and generate the corresponding radii of gyration labelled $\langle R^2_{g\perp} \rangle$ and $\langle R^2_{g\parallel} \rangle$, the sum of which equals $\langle R^2_g \rangle$. Results for the case $N = 25$ are shown in Figure 3. The perpendicular and parallel components of $\langle R^2_g \rangle$ deviate significantly from one another at low functionality and at high values of the surface interaction strength, ε^*_s. At very high values of f, the star is stiff enough to maintain the spherical shape it adopts away from the surface; this is precisely the effect observed in AFM measurements.[21] Thus, in the proximity of a surface, isotropy breaks down, and the components of $\langle R^2_g \rangle$ no longer scale like $f^{2/5}$. The strong interaction with the surface significantly alters the structure of a low- or mid-functionality adsorbed star.

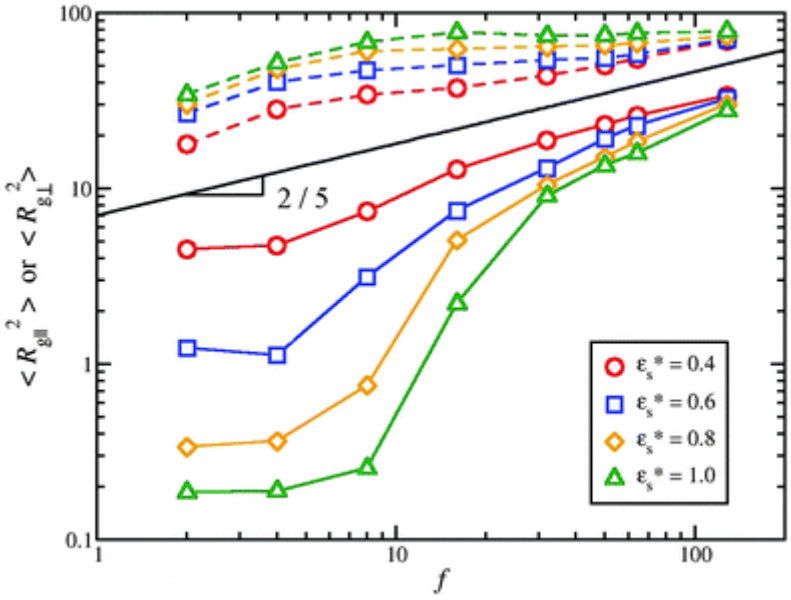

Figure 3. The parallel and perpendicular components of the squared radius of gyration, $\langle R^2_{g\parallel} \rangle$ (dashed lines) and $\langle R^2_{g\perp} \rangle$ (solid lines), respectively, as functions of functionality f, for star polymers with arm length $N = 25$ in good-solvent conditions ($\lambda = 0$). The black line corresponds to $\langle R^2_g \rangle \sim f^{2/5}$.

Figure 4 shows the ratio of the parallel component of the radius of gyration of an isolated star on the surface over its value in the bulk, $\langle R^2_{g\parallel} \rangle_0 = \frac{2}{3} \langle R^2_g \rangle_0$. This ratio signals the effects of the surface on the shape and size of the star; it is greater than 1 since the polymer spreads laterally on the surface. As

seen above, for low functionalities the star has a two-dimensional conformation and for high functionalities the star polymer regains its bulk statistics. A star polymer having a two-dimensional conformation means that we can use the scaling arguments for two-dimensional stars, *i.e.*, $\langle R^2_{g\parallel}\rangle \sim f^{1-\nu} = f^{1/4}$, [$\nu = 3/(d+2)$ in d dimensions].[37] This leads to the prediction that

$$\langle R^2_{g\parallel}\rangle \; / \; \langle R^2_{g\parallel}\rangle_0 \sim f^{1/4}/f^{2/5} = f^{-3/20} \qquad (12)$$

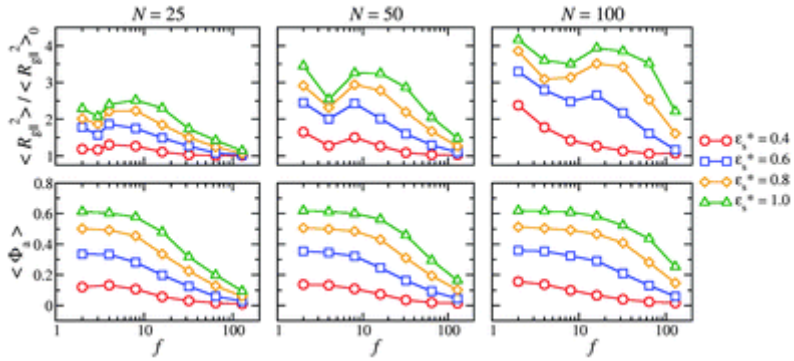

Figure 4. Properties of isolated adsorbed star polymers with arm lengths N= 25 (left column), N = 50 (middle column), and N = 100 (right column) in good-solvent conditions: (top row) the parallel component of the squared radius of gyration $\langle R^2_{g\parallel}\rangle$, divided by its value for an isolated star polymer in bulk; (bottom row) the bound fraction $\langle \Phi_a \rangle$.

However, the results in Figure 4 do not follow such a simple scaling law for all values of f. At f = 2 (equivalent to a linear chain) the ratio is greater than one, meaning that the polymer has spread out on the surface. For all N, the ratio first decreases with increasing f; this effect is more pronounced with stronger surface interactions. This suggests that, at very low functionalities, each arm of the star polymer behaves like an independent linear chain, held closely to the surface (hence the observed dependence on ε^*_s). For low values of f, each arm on the surface is well separated from the rest of the arms of the star and hence there is little or no interaction between them; as a result, $\langle R^2_{g\parallel}\rangle$ is, initially, insensitive to an increase in f. In the bulk, however, the arms are free to explore all possible conformations, and hence they interact with each other more; therefore, $\langle R^2_{g\parallel}\rangle_0$ is expected to increase. The ratio of the two therefore decreases initially, until it reaches a local minimum. The subsequent increase is due to the onset of interactions between arms on the surface: at first, these interactions simply cause a stretching of the arms on the surface, leading to an increase in $\langle R^2_{g\parallel}\rangle$. Figure 1(a) and (d) show snapshots of systems in which the arms are held flat on the surface. Eventually, though, the crowding of the arms on the surface becomes too great, and they begin to lift

from the surface. This crossover between two-dimensional and three-dimensional structures results in the ratio asymptotically approaching unity; the star's core lifts from the surface (see Figure 2) and the molecule regains bulk characteristics and shape.

The bound fraction $\langle \Phi_a \rangle$ is defined here as the average fraction of beads within a certain distance of the surface. As in our previous work,[23] this distance was determined by inspection of the bead probability density profile $p(z)$ (not shown) which shows a primary peak at a distance $z/\sigma \simeq \sqrt[6]{2/5} \simeq 0.86$ corresponding to the minimum in $V_s(z)$ [Eq. (7)], and either a local minimum or a point of inflexion at $z/\sigma \simeq 1.2$. The latter distance was taken as a criterion for assessing whether a particular bead is bound to the surface or not. $\langle \Phi_a \rangle$ is shown as a function of f in Figure 4. At low functionalities $\langle \Phi_a \rangle$ remains roughly constant at a value dictated by the surface interaction energy; in essence, the arms are adsorbed independently on to the surface. The addition of more arms creates crowding effects, however, and beyond a certain threshold value of f, some arms lift off the surface, leading to a reduction in $\langle \Phi_a \rangle$.

Our results are in conflict with a statement made by Kosmas regarding a "general rule that by increasing the compactness of the stars by increasing f while keeping the total molecular weight M constant, the number of contacts with the surface and the adsorption will increase."[16] In other words, if $f$is increased with fN held constant, then $\langle \Phi_a \rangle$ should increase. In fact, the opposite trend is seen here. For example, for systems with $fN = 400$ and$\varepsilon^*_s = 1.0$ we obtain $\langle \Phi_a \rangle$ = 0.62, 0.60, and 0.48 for 4/100, 8/50, and 16/25 stars, respectively. For systems with $fN = 800$ and $\varepsilon^*_s = 0.4$ we obtain $\langle \Phi_a \rangle$ = 0.10, 0.07, and 0.03 for 8/100, 16/50, and 32/25 stars, respectively. Kosmas found theoretically that *ideal* star polymers , ring polymers , and comb polymers each have fewer contacts than does an *ideal* linear polymer under conditions where the monomer-surface interaction was of finite strength but infinitesimally short range.[16] In a subsequent theoretical study,[38] Stratouras and Kosmas compare the adsorption of linear and ring polymers with more realistic monomer-surface interactions and confirm the opposite trend established experimentally when the adsorption was "clearly marginal".[39] By inference, with more realistic treatments of the effective monomer-monomer and monomer-surface interactions, the theoretical prediction should be that physisorbed star polymers will also possess fewer contacts than linear polymers , as is observed in our simulations.

The variations of $\langle \Phi_a \rangle$ with f shown in Figure 4 appear quite regular, which suggests that it might scale with some appropriate combination of f,N, and ε^*_s. In fact, Halperin and Joanny provide predictions for this scaling:[15] in the 2D star (strong-adsorption) regime, $\langle \Phi_a \rangle \sim \delta^{2/3}$; in the sombrero regime, $\langle \Phi_a \rangle \sim Nf^{-1}\delta^{2/3}$; and in the colloidal (weak-adsorption) regime $\langle \Phi_a \rangle \sim N^{2/5}f^{-6/5}\delta^{2/3}$. Figure 5 shows $\langle \Phi_a \rangle /(\varepsilon^*_s)^{2/3}$plotted against N/f on log-log scales. The results show that,

at high values of N/f, each system is in an apparently strong-adsorption regime where $\langle\Phi_a\rangle$ is independent of N and f. The scaling with ε^*_s (crudely identified with δ) is not in perfect agreement with the theoretical predictions; in particular, the data for $\varepsilon^*_s = 0.4$ scarcely show the predicted plateau. At smaller values of N/f, $\langle\Phi_a\rangle$ decreases; if the system crosses over from the 2D star regime to the sombrero regime, then $\langle\Phi_a\rangle$ should be proportional to N/f. Unfortunately, the data are not sufficiently detailed to discriminate between the various scaling laws predicted by Halperin and Joanny (including the scaling law appropriate to the colloidal regime). In any case, it seems unlikely that the cartoon of the sombrero regime provided by Halperin and Joanny is very precise: in their work, the core of the star polymer is in contact with the surface as part of an adsorbed disk, and the desorbed arms are free to point away from the surface in the form of a hemispherical cap;[15] from the simulations, Figure 1(b) and (e) show that the core is more likely to have lifted off from the surface, and that the cap is not a perfect hemisphere.

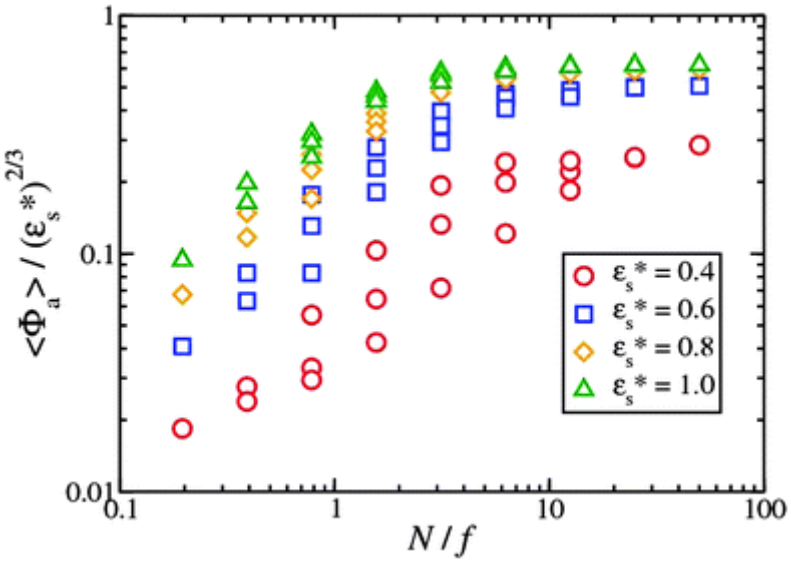

Figure 5. Bound fractions $\langle\Phi_a\rangle$ divided by $(\varepsilon^*_s)^{2/3}$ for isolated adsorbed stars on various surfaces, plotted against N/f.

The shape of a physisorbed star allows one to further understand the influence of the surface. For an overview concerning star polymers in bulk see ref. 40. One measure, developed by Rudnick *et al.*,[41] is the asphericity, A, defined as

$$A = \frac{\sum_{j>i}^{d} \left\langle \left(L_i^2 - L_j^2 \right) \right\rangle}{(d-1)\left\langle \left(\sum_{i=1}^{d} L_i^2 \right)^2 \right\rangle} \qquad (13)$$

where L_i are the principal components of the squared radius of gyration, and d is the number of the principal components (equal to the number of spatial dimensions). The quantity A has an upper bound of 1 when it is extended in one dimension (rod-like); the lower bound is 0 for a circular shape in $d = 2$ and a spherical shape in $d = 3$. Figure 6 shows A_{xyz} (three-dimensional asphericity) for a star in the bulk and on a surface with different bead-surface energies. It provides information on how much the surface has affected a star's shape. In previous studies it was found that in the bulk the asphericity drops as $\sim f^{-1}$,[40] which is in agreement with our own results for the bulk. However, the results for stars on the surface show a more complex picture. For this reason, Figure 6 also shows A_{xy}, which is the two-dimensional asphericity with the bead positions projected on to the surface. The quantity A_{xy} has a weak power-law dependence that scales with $\sim f^{-1.4}$, which is different from that found in the bulk. In addition, Figure 6 shows the asphericity in the xz plane A_{xz}, which provides a clear indication of the adsorbed star's flatness. The results show that for high values of ε^*_s and low values of f, A_{xz} has values near to 1 meaning that the star lies flat on the surface. Note that the longer the arms are, the higher the functionality is required to start regaining its three-dimensional bulk shape. Longer arms have more monomer contacts with the surface, and so a higher degree of crowding is required to tip the free-energy balance in favour of desorption. Thus one can adjust the strength of the surface interaction and the length of the arms of a star to stabilise a high-f star in a (nearly) two-dimensional conformation. A more detailed investigation of the transition between two-dimensional and three-dimensional structures is in progress.

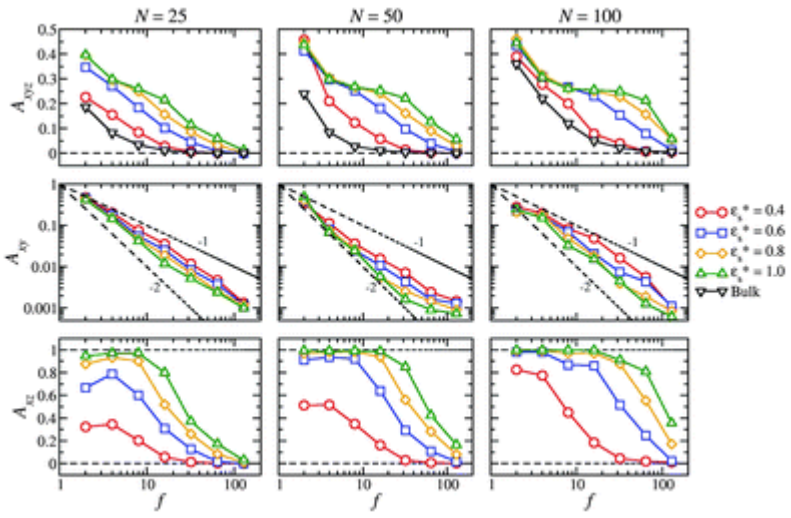

← ***Figure 6.*** Measures of asphericity for isolated adsorbed and bulk star polymers with arm lengths $N = 25$ (left column), $N = 50$ (middle column), and $N = 100$ (right column) in good-solvent conditions: (top row) three-dimensional asphericity A_{xyz}; (middle row) two-dimensional asphericityA_{xy}, in the plane of the surface; (bottom row) two-dimensional asphericityA_{xz}, in a plane perpendicular to the surface.

Four different structural regimes have been identified from the results presented above. The linear regime corresponds to the case where the arms do not interact significantly with one another, and so the star polymer acts like a network of loosely-coupled linear chains. The colloidal regime applies when the star resembles a soft colloid. The 2D star and sombrero regimes are intermediate between the linear and colloidal regimes: a 2D star extends in the lateral dimensions only, and thus resembles a true two-dimensional star polymer ; and in a sombrero structure, the star is strongly anchored to the surface by adsorbed arms, but some arms have desorbed. The boundary between the linear and 2D star regimes is identified using the first minimum in $\langle R^2_{g\parallel}\rangle / \langle R^2_{g\parallel}\rangle_0$ as a function of f, as shown in Figure 4. The transition between the 2D star and sombrero regimes occurs at the point where $\langle h_{\mathrm{core}}\rangle / \langle h\rangle$ starts to decrease significantly, signalling the desorption of arms from the surface, as shown in Figure 2. Finally, the boundary between the sombrero and colloidal regimes is identified using the minimum occurring in $\langle h_{\mathrm{core}}\rangle / \langle h\rangle$, beyond which the core lifts off from the surface. The boundaries between these regimes can be represented on a 'phase diagram'; Figure 7 shows an example for a bead-surface energy $\varepsilon^*_s = 1.0$. For the purposes of constructing this figure, additional simulations of polymers with arm lengths $N = 10$ and $N = 75$ were carried out. Increasing f with fixed N leads to the sequence linear-2D star-sombrero-colloid, while increasing N at fixed f would lead to the reverse sequence.

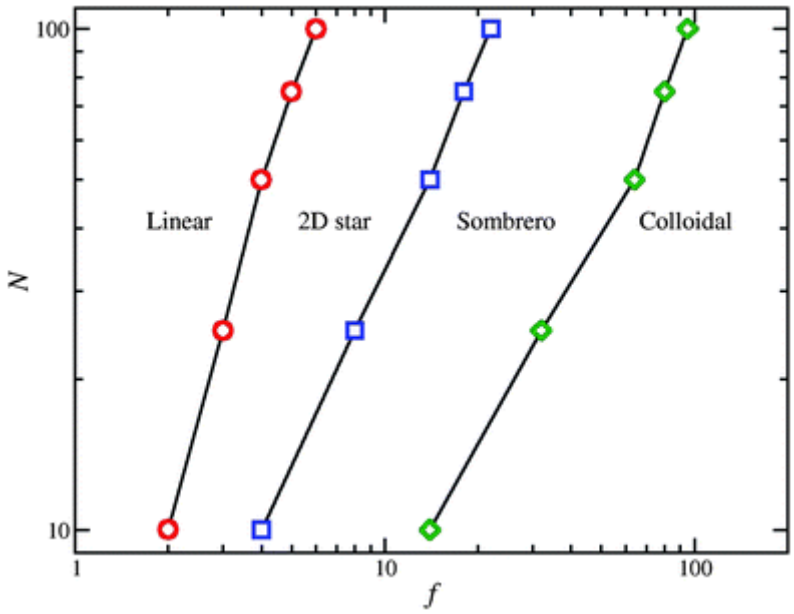

Figure 7. Structural phase diagram for isolated adsorbed star polymers with functionality f, arm length N, and bead-surface energy $\varepsilon^*_s = 1.0$, in good-solvent conditions.

B. Solvent effects on an isolated star

This section is focused on the effects of the solvent on the structure of an isolated adsorbed star polymer . These were studied by taking final configurations from the simulations performed in good-solvent conditions ($\lambda = 0$) and equilibrating the system with $0 < \lambda \leq 1$ over times of around $2 \times 10^6 \delta t$; to allow effective equilibration, λ was increased in steps of 0.1. The final values of λ considered here are 0.4, 0.646 (corresponding to θ-solvent conditions[33]), and 1. Production runs of $4 \times 10^6 \delta t$ were carried out after equilibration.

Increasing λ corresponds to increasing bead-bead attractions. The immediate result is that the star polymer shrinks in size, as illustrated in Figure 8which shows $\langle h \rangle$ and $\langle h_{\text{core}} \rangle$. Generally speaking, both quantities are reduced by decreasing the solvent quality; the polymer collapses on the surface. There is, however, an anomalous increase in $\langle h_{\text{core}} \rangle$ between $\lambda = 0.646$ and $\lambda = 1$ for the case of low bead-surface energy $\varepsilon^*_s = 0.4$. This is attributed to the bead-bead interactions dominating the bead-surface interactions, leading to the polymer adopting a more spherical conformation and the core lifting off again from the surface. This behaviour is precluded by a strong surface energy, such as $\varepsilon^*_s = 1$, which serves to anchor the core near the surface.

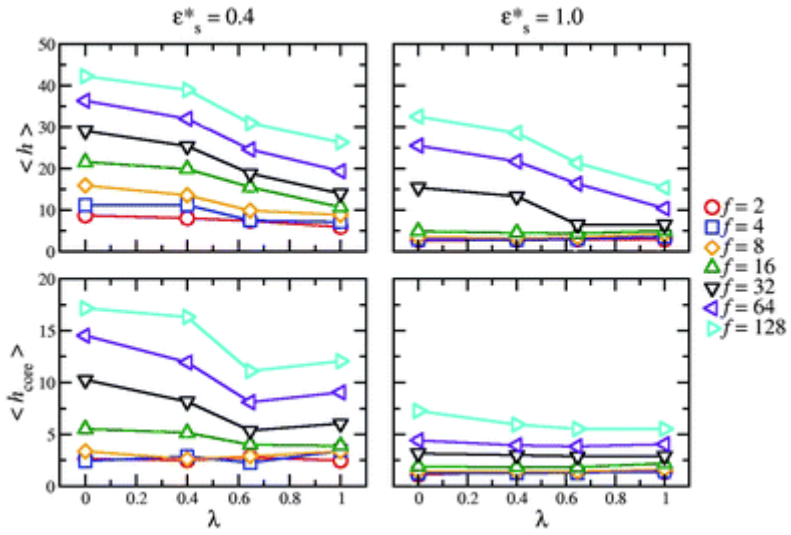

Figure 8. Dimensions of isolated star polymers with arm length $N = 50$ adsorbed on the surface with bead-surface energy $\varepsilon^*_s = 0.4$ (left column) and $\varepsilon^*_s = 1.0$ (right column) in varying solvent conditions λ: (top row) average height of the star $\langle h \rangle$; (bottom row) average core height $\langle h_{\text{core}} \rangle$.

Figure 9 shows $\langle R^2_{gl} \rangle$ and $\langle \Phi_a \rangle$. As described above, when the solvent quality is reduced, the star polymer shrinks in size. The behaviour of $\langle R^2_{gl} \rangle$ reflects this shrinking effect for both bead-surface energies considered (ε^*_s = 0.4 and 1.0). The bound fraction, however, shows some non-trivial behaviour. With ε^*_s = 0.4, $\langle \Phi_a \rangle$ remains essentially constant for all λ; the shrinking of the polymer in the lateral directions could be pictured as a kind of concertina process, where the number of contacts with the surface is conserved. With ε^*_s = 1, there is a significant decrease of $\langle \Phi_a \rangle$ as λ is increased towards 1; stronger monomer-surface interactions hold the polymer arms flatter on the surface and with more surface contacts; this increases crowding and makes it more difficult for arms to contract without losing surface contacts.

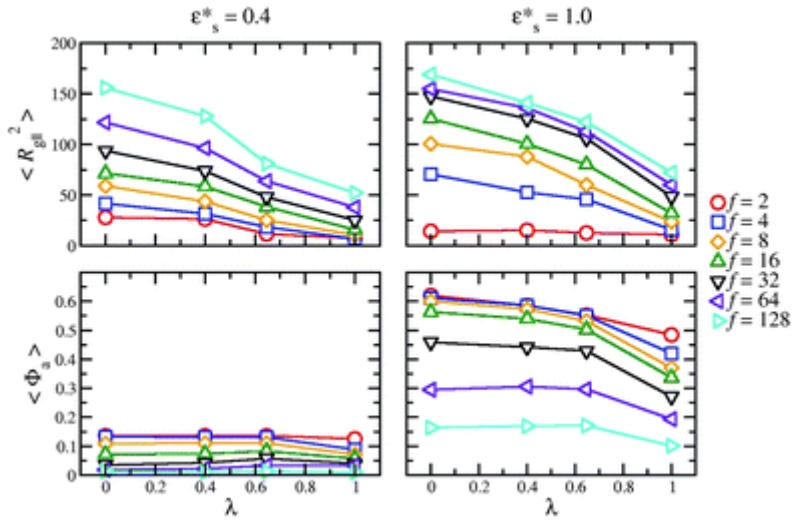

Figure 9. Properties of isolated adsorbed star polymers with arm length N = 50 adsorbed on to the surface with bead-surface energy ε^*_s = 0.4 (left column) and ε^*_s = 1.0 (right column) in varying solvent conditions λ: (top row) the parallel component of the squared radius of gyration $\langle R^2_{gl} \rangle$; (bottom row) the bound fraction $\langle \Phi_a \rangle$.

These descriptions are illustrated in Figure 10 by simulation snapshots for f/100 polymers with monomer-surface interactions of ε^*_s = 0.4 and 1.0. With ε^*_s = 0.4 the collapsed polymers adopt globular conformations, but with ε^*_s = 1.0 the stars are flatter; in addition, the structures become more regular with increasing f.

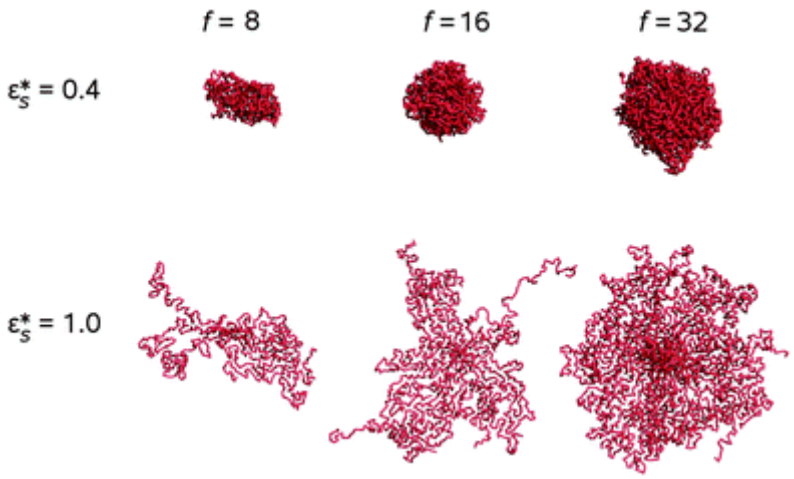

Figure 10. Top-view snapshots of *f*/100 star polymers in bad-solvent conditions, with *f* = 8 (left column), *f* = 16 (middle column), and *f* = 32 (right column): (top row) bead-surface energy $\varepsilon^*_s = 0.4$; (bottom row) $\varepsilon^*_s = 1.0$.

At this point we make contact with experiment, by comparing the structures shown in Figure 10 with those inferred from AFM measurements of dried films.[21] Figure11 (a)-(c) show AFM topography images of polybutadiene star polymers adsorbed on mica from toluene solution; the incubation times in these experiments were short so that the surface coverages are low, and hence the observed structures are essentially those of isolated molecules. (Incubation refers to the time the mica surface is held in the polymer solution, prior to rinsing and drying.) The images correspond to three different functionalities, (a) *f* = 18, (b) *f* = 32, and (c) *f* = 59. As the functionality is increased, the conformations of the star polymers become more regular, corresponding to the approach towards the colloidal regime.

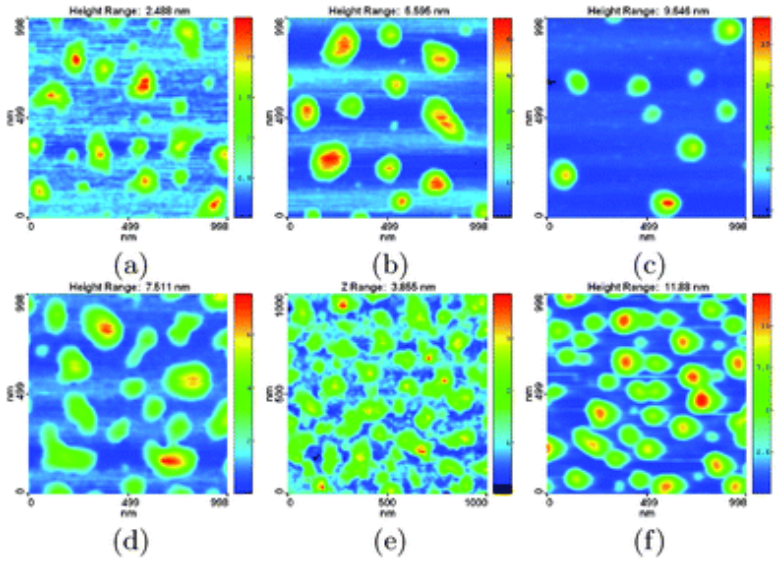

← ***Figure 11.*** AFM topography images of polybutadiene star polymers with functionality *f*, adsorbed on mica from toluene solution with incubation times *t*: (a) *f* = 18 (*t* = 5 mins); (b) *f* = 32 (*t* = 10 mins); (c) *f* = 59 (*t* = 180 mins); (d) *f* = 18 (*t* = 760 mins); (e) *f* = 32 (*t* = 1440 mins); (f) *f* = 59 (*t* = 3600 mins).

C. Many adsorbed stars in good solvent

In good-solvent conditions, polymers experience purely repulsive effective mutual interactions. Simulations with $\lambda = 0$ were initiated by preparing configurations with many polymers on a surface, and equilibrating for around $5 \times 10^6 \delta t$. The number of molecules is N_b/fN, where $N_b = 20\,000$ is the number of beads used in all simulations (excluding the core beads). To avoid finite-size artifacts, only relatively small polymers were studied: 2/25, 4/25, 8/25, and 16/25. Following equilibration, production runs of $4 \times 10^6 \delta t$ were performed. During equilibration runs at higher surface concentrations, some of the polymers were seen to desorb as the polymer film approached the steady state. Adsorption was therefore measured by the steady-state surface bead density, defined in terms of the number of beads N_{ads} belonging to those stars with at least one bead-surface contact, identified using the distance-based criterion $z \leq 1.2\sigma$. Note that N_{ads} is, in general, greater than the number of beads actually bound to the surface. The reduced surface bead density is $\rho^* = N_{\mathrm{ads}}\sigma^2/L^2$. For an *isolated* star, an effective surface bead density is defined by

$$\rho_g^* = \frac{N\sigma^2}{A_g} \qquad (14)$$

where $A_g = \pi \langle R^2_{g\mathrm{l}} \rangle$ is the area covered on the surface by the adsorbed polymer . ρ^*_g can be used to define the critical overlap concentration between star polymers . The dilute regime corresponds to $\rho^* \ll \rho^*_g$; in this regime the individual stars are almost independent from one another, and their structures are essentially those of an isolated star. For $\rho^* > \rho^*_g$, excluded-volume interactions should perturb the polymer conformations. In terms of the density parameter

$$\gamma = \frac{\rho^*}{\rho_g^*} \qquad (15)$$

the critical overlap concentration corresponds to $\gamma = 1$. By placing a number of stars on surfaces of various dimensions, it was possible to simulate up to the critical overlap concentration. In other words, the simulations were performed at surface concentrations (within the film) approaching the semidilute regime.

Figure 12 shows the behaviour of $\langle h \rangle$ and $\langle h_{\mathrm{core}} \rangle$ with varying surface density. For very small surface densities the star polymers are dispersed on the surface, and so we expect identical results with those of an isolated star polymer . (Note that $\gamma = 0$ corresponds to an isolated star.) Under weak-adsorption conditions ($\varepsilon^*_s = 0.4$) only small values of γ could be addressed due to desorption. In general, increasing the surface density leads to increases in both $\langle h \rangle$ and $\langle h_{\mathrm{core}} \rangle$; evidently, the polymers bunch up as they begin to overlap. The maximum height of the film $\langle h \rangle$ is more sensitive

to the density γ with stronger surface interactions ε^*_s. This is because the arms are held flatter on the surface, leading to more excluded-volume interactions with neighbouring polymers . The core height $\langle h_{\text{core}} \rangle$, however, is less sensitive to density with the stronger monomer-surface interaction; this interaction keeps the core more firmly anchored to the surface, outweighing the interactions between polymer arms.

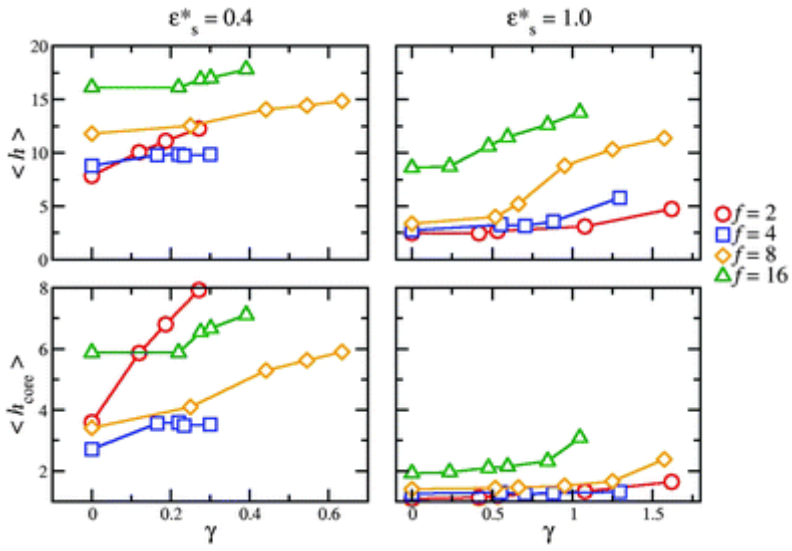

Figure 12. Dimensions of *f*/25 star polymers adsorbed on surfaces with bead-surface energy $\varepsilon^*_s = 0.4$ (left column) and $\varepsilon^*_s = 1.0$ (right column), at various relative surface densities γ: (top row) the average height of the star $\langle h \rangle$; (bottom row) the average core height $\langle h_{\text{core}} \rangle$.

Figure 13 shows the ratio of the parallel and the perpendicular components of the radius of gyration $\langle R^2_{g\parallel} \rangle$ / $\langle R^2_{g\perp} \rangle$, and the bound fraction $\langle \Phi_a \rangle$. The results show that under weak-adsorption conditions ($\varepsilon^*_s = 0.4$) the polymers bunch up but without significant changes in the bound fraction. Under strong-adsorption conditions ($\varepsilon^*_s = 1$), $\langle R^2_{g\parallel} \rangle$ / $\langle R^2_{g\perp} \rangle$ is larger for a fixed value of γ, and the bound fraction decreases significantly as the density is increased. The latter behaviour arises because the arms are held flatter on the surface and with more surface contacts, and hence the arms are less able to 'bunch up' under the influence of excluded-volume interactions without losing contacts.

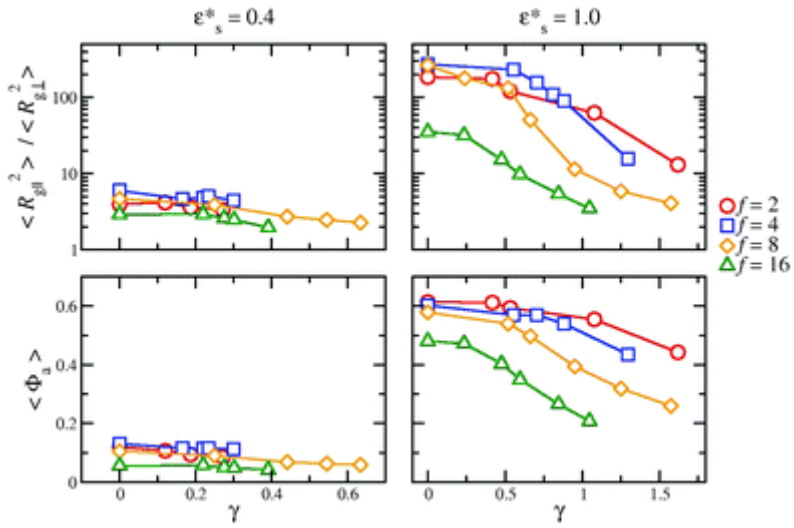

Figure 13. Properties of *f*/25 star polymers adsorbed on surfaces with bead-surface energy $\varepsilon^*_s = 0.4$ (left column) and $\varepsilon^*_s = 1.0$ (right column), at various relative surface densities γ: (top row) the ratio of the parallel and perpendicular components of the squared radius of gyration $\langle R^2_{g\parallel}\rangle$ / $\langle R^2_{g\perp}\rangle$; (bottom row) the bound fraction $\langle \Phi_a \rangle$.

D. Many adsorbed stars in bad solvent

The final step in the experimental polymer -adsorption procedure[20,21] that motivated this work is the quench from good-solvent to bad-solvent conditions (corresponding to rinsing with solvent and then drying in nitrogen /air). As described for the case of linear chains in ref. 23, this step can be mimicked in simulations by starting simulations from well-equilibrated configurations with $\lambda = 0$ (good solvent) and then instantaneously switching to $\lambda = 1$ (bad solvent). The system was re-equilibrated for $5 \times 10^6 \delta t$, during which time the system was seen to reach an apparent steady state. Experimentally, the surface structures formed from this quenching procedure are apparently stable over periods of at least months. In our simulations the structures observed are apparently static on the accessible timescales.

Figure 14 shows equilibrated simulation configurations before ($\lambda = 0$) and after ($\lambda = 1$) the quench, for systems of polymers made up from arms with $N = 25$ beads, with bead-surface energy $\varepsilon^*_s = 0.4$, with different functionalities, and at various surface densities. In good-solvent conditions the polymers are in extended conformations, but in bad-solvent conditions they collapse to optimise the attractive bead-bead interactions. Functionality plays a significant role in determining the degree of clustering between the polymers . Even at low densities, low functionalities of $f = 2$ or 4 lead to clusters composed of four or even six polymers , while for $f = 16$ one has to reach higher values of surface coverage ($\gamma \cong 0.75$) to observe a cluster composed of three polymers . The interpenetration of polymers is dictated by the stiffness of the star polymers before the quench. For low functionalities

the star polymers diffuse in the lateral directions and once they collide, they easily interpenetrate with one another. The probability of two polymers belonging to a single cluster after the quench is clearly enhanced if they interpenetrate before the quench. For higher values of *f*, the degree of interpenetration between polymers is greatly reduced due to the osmotic repulsion between the stars. Therefore high-functionality stars, prior to the quench, position themselves in such a way as to minimise the degree of overlap with one another. Hence, after the quench the star polymers tend to form isolated collapsed globules, or very rarely, small clusters. To observe clustering of high functionality star polymers, one has to increase significantly the surface density in order to promote overlap. Another important contributing factor is that the mobility decreases with increasing functionality. Therefore, the collapse of an isolated star could occur on a timescale shorter than that required for two stars to diffuse together, and so there may be a kinetic effect which militates against clustering of high-functionality stars.

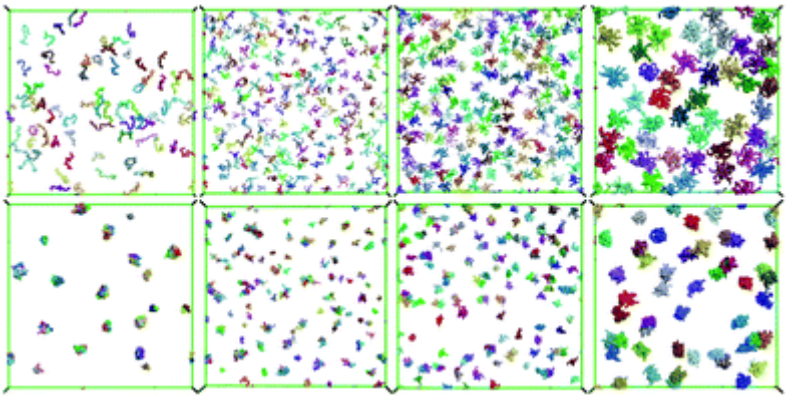

Figure 14. Top-view snapshots of *f*/25 star polymers (*f* is the functionality) adsorbed at relative surface density γ on the surface with bead-surface energy $\varepsilon^*_s = 0.4$, in good-solvent conditions (top row) and in bad-solventconditions (bottom row). From left to right (f, γ) = (2, 0.107), (4, 0.186), (8, 0.466), and (16, 0.750).

The decrease in clustering with increasing functionality has been studied in experiments, such as those conducted by us.[21] To make contact with this work, Figure 11(d)-(f) shows AFM images of polybutadiene star polymers with $f = 18$, 32, and 59, adsorbed on to mica from toluene , and then dried. The incubation times are long, meaning that the surface coverages are high enough (although still sub-monolayer) for interactions between molecules to be significant. With $f = 18$, individual molecules interpenetrate, fuse together, and cannot be distinguished within clusters , which are themselves rather irregular in shape. With $f = 32$, the distribution of molecular centres is more uniform, suggesting an increase in repulsions between the molecules; the *apparent* overlap of

individual molecules should not be interpreted as evidence for clustering, however, because AFM tip - convolution effects limit the resolution of the topography images. Finally, with $f = 59$, individual molecules can clearly be resolved, and almost no association can be observed. These structures are taken in air, which is considered a 'bad solvent '. Hence, it is meaningful to compare these experimental images with the simulation snapshots in Figure 14. There is excellent accord: the simulations successfully reproduce the decrease in clustering with increasing functionality, as observed in experiments.

4. Conclusion

In this work Langevin dynamics simulations of coarse-grained, bead-spring models have been used to gain insight on the adsorption of star polymerson to a smooth surface. The study was motivated by experimental AFM images of polymers physisorbed from solution on to mica surfaces followed by solvent evaporation. The process was mimicked by switching the coarse-grained model interactions between those appropriate for good-solvent and bad-solvent conditions.

Of particular interest was the observation of the crossover from polymer -like to colloidal behaviour. For isolated polymers in good-solvent conditions, three parameters were identified as being important for controlling the structure of the star on the surface: the functionality, the arm length, and the bead-surface energy. By exploring this parameter space, four different structural regimes were identified: the linear regime at low functionality, where the polymer arms behave essentially independent of one another; the 2D star regime, where the polymer behaves like a true two-dimensional molecule; the sombrero regime, characterized by a strong adsorbed disk with a central cap (as predicted by theory[15]); and the colloidal regime, where the polymer adopts a roughly (hemi)spherical conformation. These regimes were mapped onto a phase diagram; in this work, the functionality-arm length plane was selected, at constant bead-surface energy.

The simulation methodology allows the solvent quality to be tuned with a single parameter, thus gaining valuable insights on the conformational changes likely to be induced by solvent . The collapse of isolated stars on a surface with decreasing solvent quality was considered, and then the quench of a many-polymer system from good-solvent conditions to bad-solvent conditions was examined. The observed structures are in good qualitative agreement with those observed in AFM experiments, and can be rationalized in terms of the probable interpenetration between polymers before the quench.

References

[1] M. Daoud and J. P. Cotton, *J. Phys. (France)*, 1982, **43**, 531–538.

[2] T. M. Birshtein and E. B. Zhulina, *Polymer*, 1984, **25**, 1453–1461.

[3] T. M. Birshtein, E. B. Zhulina and V. O. Borisov, *Polymer*, 1986, **27**, 1078–1086.

[4] K. Šolc and W. H. Stockmayer, *J. Chem. Phys.*, 1971, **54**, 2756–2757.

[5] K. Šolc, *J. Chem. Phys.*, 1971, **55**, 335–344.

[6] K. Šolc, *Macromolecules*, 1973, **6**, 378–385.

[7] J. Batoulis and K. Kremer, *Macromolecules*, 1989, **22**, 4277–4285.

[8] G. Zifferer, *J. Chem. Phys.*, 1999, **110**, 4668–4677.

[9] S. Asakura and F. Oosawa, *J. Polym. Sci.*, 1958, **33**, 183–192.

[10] S. M. Ilett, A. Orrock, W. C. K. Poon and P. N. Pusey, *Phys. Rev. E*, 1995, **51**, 1344–1352.

[11] J. Dzubiella, C. N. Likos and H. Löwen, *J. Chem. Phys.*, 2002, **116**, 9518–9530.

[12] K. Ohno and K. Binder, *J. Chem. Phys.*, 1991, **95**, 5444–5458.

[13] K. Ohno and K. Binder, *J. Chem. Phys.*, 1991, **95**, 5459–5473.

[14] J. F. Joanny and A. Johner, *J. Phys. II*, 1996, **6**, 511–527.

[15] A. Halperin and J. F. Joanny, *J. Phys. II*, 1991, **1**, 623–636.

[16] M. K. Kosmas, *Macromolecules*, 1990, **23**, 2061–2065.

[17] K. Shida, K. Ohno, M. Kimura and Y. Kawazoe, *J. Chem. Phys.*, 1996, **105**, 8929–8936.

[18] G. Kritikos and A. F. Terzis, *Polymer*, 2008, **49**, 3601–3609.

[19] I. Hiotelis, A. G. Koutsioubas, N. Spiliopoulos, D. L. Anastassopoulos, A. A. Vradis, C. Toprakcioglu, A. Menelle, G. Sakellariou and N. Hadjichristidis, *Macromolecules*, 2008, **41**, 7648–7655.

[20] E. Glynos, A. Chremos, G. Petekidis, P. J. Camp, E. Theofanidou, and V. Koutsos (unpublished)

[21] E. Glynos, A. Chremos, G. Petekidis, P. J. Camp and V. Koutsos, *Macromolecules*, 2007, **40**, 6947–6958.

[22] A. Kiriy, G. Gorodyska, S. Minko, M. Stamm and C. Tsitsilianis, *Macromolecules*, 2003, **36**, 8704–8711.

[23] A. Chremos, E. Glynos, V. Koutsos and P. J. Camp, *Soft Matter*, 2009, **5**, 637–645.

[24] G. S. Grest, K. Kremer and T. A. Witten, *Macromolecules*, 1987, **20**, 1376–1383.

[25] G. S. Grest, *Macromolecules*, 1994, **27**, 3493–3500.

[26] S. Huissmann, R. Blaak and C. N. Likos, *Macromolecules*, 2009, **42**, 2806–2816.

[27] C. N. Likos, H. Löwen, M. Watzlawek, B. Abbas, O. Jucknischke, J. Allgaier and D. Richter, *Phys. Rev. Lett.*, 1998, **80**, 4450–4453.

[28] A. Sikorski, *Macromol. Theory Simul.*, 2001, **10**, 38–45.

[29] A. Sikorski, *Macromol. Theory Simul.*, 2003, **12**, 325–331.

[30] M. Konieczny and C. N. Likos, *Soft Matter*, 2007, **3**, 1130–1134.

[31] G. S. Grest and K. Kremer, *Phys. Rev. A*, 1986, **33**, 3628–3631.

[32] S. W. Sides, G. S. Grest and M. J. Stevens, *Macromolecules*, 2002, **35**, 566–573.

[33] M. O. Steinhauser, *J. Chem. Phys.*, 2005, **122**, 094901.

[34] J. D. Weeks, D. Chandler and H. C. Andersen, *J. Chem. Phys.*, 1971, **54**, 5237–5247.

[35] M. P. Allen and D. J. Tildesley, *Computer simulation of liquids*, Clarendon Press, Oxford, 1987.

[36] A. Jusufi, J. Dzubiella, C. N. Likos, C. von Ferber and H. Löwen, *J. Phys.: Condens. Matter*, 2001, **13**, 6177–6194.

[37] P. G. de Gennes, *Scaling Concepts in Polymer Physics*, Cornell University Press, Cornell, 1979.

[38] G. Stratouras and M. Kosmas, *Macromolecules*, 1992, **25**, 3307–3308.

[39] R. Yerushalmi-Rozen, B. J. Hostetter, L. J. Fetters and J. Klein, *Macromolecules*, 1990, **23**, 2984–2987.

[40] G. Zifferer, *J. Chem. Phys.*, 1995, **102**, 3720–3726.

[41] J. Rudnick and G. Gaspari, *Science*, 1987, **237**, 384–389.